NIC

Time-Dependent Density Functional Theory

Nikos L. Doltsinis

http://www.fz-juelich.de/nic-series/volume31

Time-Dependent Density Functional Theory

Nikos L. Doltsinis

Chair of Theoretical Chemistry
Ruhr-Universität Bochum
44780 Bochum, Germany
E-mail: nikos.doltsinis@theochem.rub.de

Time-dependent density functional theory (TDDFT) is the generalization of stationary DFT to time-dependent potentials and electron densities. Most practical applications are concerned with the interaction of molecules with an electric laser field. In the vast majority of cases, such as the calculation of photoabsorption spectra for fixed nuclei, the electric field constitutes a small perturbation which can be treated using linear response theory. This has to be distinguished from directly solving the time-dependent Kohn-Sham equations in the time domain, i.e. dynamically propagating orbitals and nuclei.

1 Introduction

Density functional theory (DFT) in its usual time-independent form is essentially a ground state theory and, as such, excludes the interaction of matter with time-dependent fields. There is generally no rigorous way, for example, to calculate electronic excitation energies due to photoabsorption. Standard DFT can be extended to excited states representing the lowest state of a given space-spin symmetry. Beyond this, a number of *ad hoc* solutions based on Ziegler's sum method[1] have been proposed over the years[2–13].

The description of time-dependent phenomena, including photoexcitation, was incorporated properly into DFT by Runge and Gross[14] who generalized the Hohenberg-Kohn theorem to time-dependent densities and potentials. It makes sense to distinguish between two main types of time-dependent DFT (TDDFT) calculations. The overwhelming majority of applications deal with relatively weak electric fields, e.g. photoabsorption spectra, which can be treated as a small perturbation within linear response theory. The other branch solves the TDDFT equations in the time domain to dynamically propagate electrons and nuclei[15–20]. In the present article we will limit the discussion to the linear response aspect, the particular focus being on electronic excitation.

The past decade has seen TDDFT linear response theory[14, 21–24] become the most widely used electronic structure method for calculating vertical electronic excitation energies[25, 26]. Except for certain well-known problem cases such as, for instance, charge transfer[27–30] Rydberg states[31–34] and double excitations[35], TDDFT excitation energies are generally remarkably accurate, typically to within a fraction of an electron Volt[36–38, 31].

Excited state analytical nuclear forces within TDDFT have only been implemented recently[39–42] in an attempt to extend the applicability of TDDFT beyond single point calculations. One complication has been the fact that TDDFT merely provides excitation energies, but excited state wave functions are not properly defined. The first excited state geometry optimization using analytical gradients was presented by van Caillie and Amos based on a Handy-Schaefer Z-vector method[39, 40]. An extended Lagrangian ansatz was chosen by Furche and Ahlrichs[41] and Hutter[42] for their Gaussian-type basis set and plane

wave/pseudopotential implementations, respectively. The latter variant is of particular importance for condensed phase applications since it is used in conjunction with periodic boundary conditions. In order to ensure completeness, the number of Kohn-Sham (KS) orbitals included in constructing the response matrix in a molecular orbital (MO) basis must equal the number of basis functions. Since a plane wave basis typically consists of two orders of magnitude more basis functions than a Gaussian-type basis set a complete MO formulation of TDDFT is impractical. A solution to this problem is to cast the working matrix equations directly into a plane wave basis as proposed by Hutter[42]. Earlier, Doltsinis and Sprik[43] have proposed an alternative, *active space* approach to TDDFT in which only a subset of (active) KS orbitals is selected to construct the response matrix. For a large variety of excited states, convergence of the corresponding excitation energies has been shown to be rapid with respect to the number of orbitals included in the active space[43, 30]. Doltsinis and Kosov[44] followed this active space ansatz and derived analytical expressions for excited state nuclear forces within an MO basis. In contrast to previous work, they do not rely on a Lagrangian formulation[41, 42, 45], but employ an implicit differentiation scheme instead.

This article is organized as follows. First a general introduction to TDDFT is given before deriving the working equations of TDDFT linear response theory for the calculation of excitation energies. Subsequently, we present two routes to computing excited state nuclear gradients within TDDFT linear response theory, the popular extended Lagrangian ansatz and the implicit differentiation method. Finally, we discuss some illustrative examples of excited state energy and gradient calculations using a plane wave basis set.

2   Theory

2.1   Time-Dependent Kohn-Sham Theory

According to the Runge-Gross theorem[14] there is a one to one correspondence between the time-dependent external potential, $v_{\text{ext}}(\mathbf{r}, t)$, and the time-dependent electron density, $\rho(\mathbf{r}, t)$ for a fixed initial state. This can be seen as a generalization of the usual Hohenberg-Kohn theorem[46] for electronic ground states. Similar to the static case, one can cast the many-electron problem into the Kohn-Sham non-interacting electrons form assuming non-interacting v-representability. The latter assumption means that the density of the interacting system can be reproduced by the non-interacting potential v_{s}, i.e.

$$\rho(\mathbf{r}, t) = \sum_i^{\text{occ}} |\phi_i(\mathbf{r}, t)|^2 \qquad (1)$$

where the orbitals $\phi_i(\mathbf{r}, t)$ satisfy the time-dependent Kohn-Sham equations

$$i\frac{\partial}{\partial t}\phi_i(\mathbf{r}, t) = \left(-\frac{\nabla^2}{2} + v_{\text{s}}[\rho](\mathbf{r}, t)\right)\phi_i(\mathbf{r}, t) \qquad (2)$$

with

$$v_{\text{s}}[\rho](\mathbf{r}, t) = v_{\text{ext}}(\mathbf{r}, t) + \int d\mathbf{r}' \frac{\rho(\mathbf{r}', t)}{|\mathbf{r} - \mathbf{r}'|} + v_{\text{xc}}[\rho](\mathbf{r}, t) \qquad (3)$$

defining the exchange-correlation potential $v_{\mathrm{xc}}[\rho](\mathbf{r}, t)$. In the usual adiabatic approximation[47], the exchange-correlation potential is taken to be simply the derivative of the static ground state exchange-correlation energy, E_{xc}, with respect to the density,

$$v_{\mathrm{xc}}[\rho](\mathbf{r}, t) \approx \frac{\delta E_{\mathrm{xc}}[\rho]}{\delta \rho} \quad . \tag{4}$$

2.2 Linear Response Theory

Let us suppose a time-dependent perturbing potential $v_1(\mathbf{r}, t)$, for instance an oscillating electric field $v_1(\mathbf{r}, t) = Ez \cos wt$, is switched on at time $t = t_0$. The external potential is then given by

$$v_{\mathrm{ext}}(\mathbf{r}, t) = v_0(\mathbf{r}) + v_1(\mathbf{r}, t) = \begin{cases} v_0(\mathbf{r}) & , t \leq t_0 \\ v_0(\mathbf{r}) + Ez \cos wt & , t > t_0 \end{cases} \tag{5}$$

where v_0 is usually the attractive Coulomb potential between electrons and nuclei

$$v_0(\mathbf{r}) = -\sum_{K}^{N} \frac{Z_K}{|\mathbf{R}_K - \mathbf{r}|} \quad . \tag{6}$$

The first order density response for *interacting* particles to the perturbation (the first order deviation of the time-dependent density $\rho(\mathbf{r}, t)$ from the unperturbed ground state density $\rho_0(\mathbf{r})$) may be obtained from,

$$\rho(\mathbf{r}, t) - \rho_0(\mathbf{r}) \approx \rho_1(\mathbf{r}, t) = \int dt' \int d\mathbf{r}' \chi(\mathbf{r}, t, \mathbf{r}', t') v_1(\mathbf{r}', t') \tag{7}$$

with the *interacting* response function

$$\chi(\mathbf{r}, t, \mathbf{r}', t') = \left. \frac{\delta \rho(\mathbf{r}, t)}{\delta v_{\mathrm{ext}}(\mathbf{r}', t')} \right|_{v_0} \quad . \tag{8}$$

Expressing the rhs of Eq. (7) in terms of the Kohn-Sham response function of *non-interacting* particles,

$$\chi_{\mathrm{s}}(\mathbf{r}, t, \mathbf{r}', t') = \left. \frac{\delta \rho(\mathbf{r}, t)}{\delta v_{\mathrm{s}}(\mathbf{r}', t')} \right|_{v_{\mathrm{s}}[\rho_0]} \tag{9}$$

one arrives at

$$\rho_1(\mathbf{r}, t) = \int dt' \int d\mathbf{r}' \chi_{\mathrm{s}}(\mathbf{r}, t, \mathbf{r}', t') v_{\mathrm{s},1}(\mathbf{r}', t') \tag{10}$$

where

$$v_{\mathrm{s},1}(\mathbf{r}, t) = v_1(\mathbf{r}, t) + \int d\mathbf{r}' \frac{\rho(\mathbf{r}', t)}{|\mathbf{r} - \mathbf{r}'|} + \int d\mathbf{r}' \int dt' f_{\mathrm{xc}}[\rho_0](\mathbf{r}, t, \mathbf{r}', t') \rho_1(\mathbf{r}', t') \tag{11}$$

with the exchange-correlation kernel

$$f_{\mathrm{xc}}[\rho_0](\mathbf{r}, t, \mathbf{r}', t') = \frac{\delta v_{\mathrm{xc}}[\rho](\mathbf{r}, t)}{\delta \rho(\mathbf{r}', t')} \quad . \tag{12}$$

3

The frequency-dependent linear density response is obtained by Fourier transform as

$$\rho_1(\mathbf{r}, \omega) = \int d\mathbf{r}' \chi_{\mathrm{s}}(\mathbf{r}, \mathbf{r}'; \omega) v_1(\mathbf{r}', \omega)$$

$$+ \int d\mathbf{r}' \int d\mathbf{r}'' \chi_{\mathrm{s}}(\mathbf{r}, \mathbf{r}'; \omega) \left(\frac{1}{|\mathbf{r}' - \mathbf{r}''|} + f_{\mathrm{xc}}[\rho_0](\mathbf{r}', \mathbf{r}''; \omega) \right) \rho_1(\mathbf{r}'', \omega) \quad (13)$$

and

$$\chi_{\mathrm{s}}(\mathbf{r}, \mathbf{r}'; \omega) = \sum_{ph} \left(\frac{\phi_p(\mathbf{r})\phi_h^*(\mathbf{r})\phi_p^*(\mathbf{r}')\phi_h(\mathbf{r}')}{\omega - (\epsilon_p - \epsilon_h)} - \frac{\phi_p^*(\mathbf{r})\phi_h(\mathbf{r})\phi_p(\mathbf{r}')\phi_h^*(\mathbf{r}')}{\omega + (\epsilon_p - \epsilon_h)} \right) \quad (14)$$

ϕ_p and ϕ_h being the Kohn-Sham particle (unoccupied) and hole (occupied) molecular orbitals corresponding to the Kohn-Sham energies ϵ_p and ϵ_h, respectively.

Equation (13) for the first-order density has to be solved self-consistently. This is most conveniently done by casting Eq. (13) into a matrix eigenvalue problem[21,22]. For this purpose, Bauernschmitt and Ahlrichs[22] parametrized the first-order density

$$\rho_1(\mathbf{r}, \omega) = \sum_{ph\sigma} \left[P_{ph\sigma}(\omega)\phi_{p\sigma}(\mathbf{r})\phi_{h\sigma}^*(\mathbf{r}) + P_{hp\sigma}(\omega)\phi_{p\sigma}^*(\mathbf{r})\phi_{h\sigma}(\mathbf{r}) \right] \quad . \quad (15)$$

Notice that we have now introduced the spin index $\sigma(=\uparrow, \downarrow)$ and the undetermined expansion coefficients $P_{ph\sigma}(\omega)$ have the meaning of the linear response of the density matrix. Equation (13) can then be rewritten as

$$\left[\begin{pmatrix} \mathbf{L} & \mathbf{M} \\ \mathbf{M}^* & \mathbf{L}^* \end{pmatrix} - \omega \begin{pmatrix} -\mathbf{1} & \mathbf{0} \\ \mathbf{0} & \mathbf{1} \end{pmatrix} \right] \begin{pmatrix} \mathbf{X} \\ \mathbf{Y} \end{pmatrix} = -v_{1,t}(\omega) \begin{pmatrix} \mathbf{V} \\ \mathbf{V}^* \end{pmatrix} \quad (16)$$

with the vector components $X_{hp\sigma} = P_{hp\sigma}(\omega), Y_{hp\sigma} = P_{ph\sigma}(\omega)$, and

$$V_{hp\sigma} = \int d\mathbf{r} \phi_{h\sigma}^*(\mathbf{r}) v_{1,\mathbf{r}}(\mathbf{r}) \phi_{p\sigma}(\mathbf{r}) \quad (17)$$

having separated the time-dependent perturbing potential into a purely space-dependent and a purely time-dependent part, i.e. $v_1(\mathbf{r}, t) = v_{1,\mathbf{r}}(\mathbf{r})v_{1,t}(t)$. The matrices $\mathbf{M}$ and $\mathbf{L}$ are given by

$$L_{hp\sigma, h'p'\sigma'} = \delta_{\sigma\sigma'}\delta_{pp'}\delta_{hh'}(\epsilon_{p\sigma} - \epsilon_{h\sigma}) + K_{hp\sigma, h'p'\sigma'} \quad (18)$$

and

$$M_{hp\sigma, h'p'\sigma'} = K_{hp\sigma, h'p'\sigma'} \quad (19)$$

with the coupling matrix

$$K_{hp\sigma, h'p'\sigma'} = \int d\mathbf{r} \int d\mathbf{r}' \phi_{h\sigma}^*(\mathbf{r})\phi_{p\sigma}(\mathbf{r}) f_{\mathrm{H,xc}}^{\sigma\sigma'}(\mathbf{r}, \mathbf{r}') \phi_{h'\sigma'}^*(\mathbf{r}')\phi_{p'\sigma'}(\mathbf{r}') \quad . \quad (20)$$

Here we have summarized the Hartree term and the exchange-correlation term in the response kernel

$$f_{\mathrm{H,xc}}^{\sigma\sigma'}(\mathbf{r}, \mathbf{r}') = \frac{1}{|\mathbf{r} - \mathbf{r}'|} + \frac{\delta^2 E_{\mathrm{xc}}}{\delta\rho^\sigma(\mathbf{r})\delta\rho^{\sigma'}(\mathbf{r}')} \quad . \quad (21)$$

The poles of the response function (Eq. (8)) of the *interacting* system represent electronic excitation energies[21,48,16]. They are characterized by zero eigenvalues of the matrix on

4

the lhs of Eq. (16) and can therefore be obtained by solving the non-Hermitian eigenvalue problem

$$\begin{pmatrix} \mathbf{L} & \mathbf{M} \\ \mathbf{M}^* & \mathbf{L}^* \end{pmatrix} \begin{pmatrix} \mathbf{X} \\ \mathbf{Y} \end{pmatrix} = \omega \begin{pmatrix} -1 & 0 \\ 0 & 1 \end{pmatrix} \begin{pmatrix} \mathbf{X} \\ \mathbf{Y} \end{pmatrix} \quad . \tag{22}$$

In the following, we shall assume the Kohn-Sham orbitals to be real. It is then possible to halve the dimension of the non-Hermitian eigenvalue problem by means of a unitary transformation[49]. The essential steps are multiplication of Eq. (22) on the left by $\begin{pmatrix} \mathbf{L} & \mathbf{M} \\ \mathbf{M} & \mathbf{L} \end{pmatrix} \begin{pmatrix} -1 & 0 \\ 0 & 1 \end{pmatrix}$ and substitution of Eq. (22) into the rhs of the resulting matrix equation. Subtracting the two equations obtained this way from each other, one finds

$$(\mathbf{L} - \mathbf{M})(\mathbf{L} + \mathbf{M})(\mathbf{X} + \mathbf{Y}) = \omega^2 (\mathbf{X} + \mathbf{Y}) \quad . \tag{23}$$

If $(\mathbf{L} - \mathbf{M})$ is positive definite, Eq. (23) can be multiplied on the left with $(\mathbf{L} - \mathbf{M})^{-\frac{1}{2}}$ yielding the Hermitian eigenvalue problem

$$\mathbf{\Omega} \mathbf{F} = \omega^2 \mathbf{F} \tag{24}$$

where

$$\mathbf{\Omega} = (\mathbf{L} - \mathbf{M})^{\frac{1}{2}} (\mathbf{L} + \mathbf{M}) (\mathbf{L} - \mathbf{M})^{\frac{1}{2}} \tag{25}$$

and

$$\mathbf{F} = (\mathbf{L} - \mathbf{M})^{-\frac{1}{2}} (\mathbf{X} + \mathbf{Y}) \tag{26}$$

The Hermitian coupling matrix (Eq. (25)) elements are

$$\Omega_{hp\sigma,h'p'\sigma'} = \delta_{\sigma\sigma'} \delta_{pp'} \delta_{hh'} (\epsilon_{p\sigma} - \epsilon_{h\sigma})^2 + 2\sqrt{\epsilon_{p\sigma} - \epsilon_{h\sigma}} K_{ph\sigma,p'h'\sigma'} \sqrt{\epsilon_{p'\sigma} - \epsilon_{h'\sigma}} \quad . \tag{27}$$

The Tamm-Dancoff approximation, which amounts to setting $\mathbf{Y}$ to zero, further simplifies the problem in particular when hybrid Hartree-Fock/DFT exchange-correlation functionals are used[35]. However, it does not reduce the computational cost or storage space compared to the full Hermitian formulation (Eq. (24)).

2.3 Excited State Gradients

Excited state analytical nuclear forces within TDDFT have only been implemented recently[39–42, 44] in an attempt to extend the applicability of TDDFT beyond single point calculations. One complication has been the fact that TDDFT merely provides excitation energies, but excited state wave functions are not properly defined. The first excited state geometry optimization using analytical gradients was presented by van Caillie and Amos based on a Handy-Schaefer Z-vector method[39, 40]. An extended Lagrangian ansatz was chosen by Furche and Ahlrichs[41] and Hutter[42] for their Gaussian-type basis set and plane wave/pseudopotential implementations, respectively. The latter variant is of particular importance for condensed phase applications since it is used in conjunction with periodic boundary conditions.

2.3.1 Extended Lagrangian Method

The starting point for the derivation of TDDFT excited state energy gradients is the construction of the extended Lagrangian[41, 42]

$$\mathcal{L} = \mathcal{L}^{\mathrm{LR}} + \mathcal{L}^{\mathrm{KS}} \tag{28}$$

consisting of the TDDFT linear response Lagrangian

$$\mathcal{L}^{\mathrm{LR}} = \langle \mathbf{X}, \mathbf{Y} | \mathbf{\Lambda} | \mathbf{X}, \mathbf{Y} \rangle - \omega \left[\langle \mathbf{X}, \mathbf{Y} | \mathbf{\Delta} | \mathbf{X}, \mathbf{Y} \rangle - 1 \right] \tag{29}$$

with

$$\mathbf{\Lambda} = \begin{pmatrix} \mathbf{L} & \mathbf{M} \\ \mathbf{M} & \mathbf{L} \end{pmatrix} \tag{30}$$

and

$$\mathbf{\Delta} = \begin{pmatrix} -\mathbf{1} & \mathbf{0} \\ \mathbf{0} & \mathbf{1} \end{pmatrix} \quad . \tag{31}$$

The corresponding non-Hermitian linear response problem (Eq. (22)) can be recovered from

$$\frac{\delta \mathcal{L}^{\mathrm{LR}}}{\delta \langle \mathbf{X}, \mathbf{Y} |} = 0 \tag{32}$$

subject to the constraint

$$\frac{\partial \mathcal{L}^{\mathrm{LR}}}{\partial \omega} = 0 \quad . \tag{33}$$

The ground state Kohn-Sham contribution is given by

$$\mathcal{L}^{\mathrm{KS}} = \sum_{ph\sigma} Z_{ph\sigma} H_{ph\sigma} - \sum_{ij} W_{ij\sigma} \left[\langle \phi_{i\sigma} | \phi_{j\sigma} \rangle - \delta_{ij} \right] \tag{34}$$

where the $Z_{ph\sigma}$ and $W_{ij\sigma}$ are Lagrange multipliers and $H_{ph\sigma}$ are matrix elements of the static Kohn-Sham Hamiltonian. The conditions

$$\frac{\partial \mathcal{L}^{\mathrm{KS}}}{\partial Z_{ph\sigma}} = 0 \tag{35}$$

and

$$\frac{\partial \mathcal{L}^{\mathrm{KS}}}{\partial W_{ij\sigma}} = 0 \tag{36}$$

ensure that the orbitals $\phi_{i\sigma}$ are orthonormal and satisfy the ground state Kohn-Sham equations. The important step is now to determine the unknown Lagrange multipliers $Z_{ph\sigma}$ and $W_{ij\sigma}$ from

$$\frac{\delta \mathcal{L}}{\delta \phi_{i\sigma}} = 0 \quad . \tag{37}$$

The derivative of the excitation energy with respect to the nuclear coordinate R_α $(\alpha = 1, \ldots, 3N)$ for a molecule consisting of N atoms yields

$$\omega^\alpha = \mathcal{L}^\alpha = \langle \mathbf{X}, \mathbf{Y} | \mathbf{\Lambda}^\alpha | \mathbf{X}, \mathbf{Y} \rangle + \sum_{ph\sigma} Z_{ph\sigma} H_{ph\sigma}^\alpha - \sum_{ij} W_{ij\sigma} \left[\langle \phi_{i\sigma}^\alpha | \phi_{j\sigma} \rangle + \langle \phi_{i\sigma} | \phi_{j\sigma}^\alpha \rangle \right] \tag{38}$$

where we have used the short-hand notation $\frac{df}{dR_\alpha} \equiv f^\alpha$ for a general function f.

2.3.2 Implicit Differentiation Approach

An alternative to the above extended Lagrangian method is the recently proposed implicit differentiation scheme[44]. In the following detailed derivation, we confine ourselves to singlet excitations (extension to triplet excitations is straightforward) and therefore drop the spin index σ.

Multiplying Eq. (24) by $\langle \mathbf{F} |$ from the left we obtain

$$\langle \mathbf{F} | \mathbf{\Omega} | \mathbf{F} \rangle = \omega^2 \quad . \tag{39}$$

Differentiation with respect to nuclear position yields

$$\omega^\alpha = \frac{1}{2\omega} \langle \mathbf{F} | \mathbf{\Omega}^\alpha | \mathbf{F} \rangle = \frac{1}{2\omega} \sum_{ph} \sum_{p'h'} F_{ph} \Omega^\alpha_{ph,p'h'} F_{p'h'} \quad , \tag{40}$$

where the F_{ph} are the components of the linear response eigenvector $\mathbf{F}$. Carrying out the differentiation of the response matrix, Eq. (40) becomes

$$\omega^\alpha = \frac{1}{\omega} \left[\sum_{ph} (F_{ph})^2 (\epsilon_p^\alpha - \epsilon_h^\alpha)(\epsilon_p - \epsilon_h) \right.$$

$$+ 2 \int d\mathbf{r} \int d\mathbf{r}' \Gamma_1(\mathbf{r}) f_{\mathrm{H,xc}}(\mathbf{r}, \mathbf{r}') \Gamma_2(\mathbf{r}')$$

$$\left. + 2 \int d\mathbf{r} \Gamma_1(\mathbf{r}) \frac{\delta^3 E_{\mathrm{xc}}}{\delta \rho(\mathbf{r})^3} \rho^\alpha(\mathbf{r}) \Gamma_1(\mathbf{r}) \right] \quad . \tag{41}$$

Here we have defined the contracted densities

$$\Gamma_1(\mathbf{r}) = \sum_{ph} F_{ph} \sqrt{\epsilon_p - \epsilon_h} \Gamma_{ph}(\mathbf{r}) \tag{42}$$

and

$$\Gamma_2(\mathbf{r}) = \sum_{ph} F_{ph} \left[\frac{\epsilon_p^\alpha - \epsilon_h^\alpha}{\sqrt{\epsilon_p - \epsilon_h}} \Gamma_{ph}(\mathbf{r}) + 2\sqrt{\epsilon_p - \epsilon_h} \Gamma_{ph}^\alpha(\mathbf{r}) \right] \tag{43}$$

with

$$\Gamma_{ij}(\mathbf{r}) = \phi_i(\mathbf{r}) \phi_j(\mathbf{r}) \quad . \tag{44}$$

In order to compute the excitation energy gradient (Eq. (41)), we require the nuclear derivatives of KS orbital energies and wave functions, ϵ_i^α and ϕ_i^α ($i = p, h$). These can be obtained using an implicit differentiation scheme as follows. We start by writing down the KS equations in matrix form

$$F_{ij} \equiv H_{ij} - \epsilon_i \delta_{ij} = 0 \quad . \tag{45}$$

For the full differential of F_{ij} we have

$$dF_{ij} = \left(\frac{\partial H_{ij}}{\partial R_\alpha} - \epsilon_i^\alpha \delta_{ij} \right) dR_\alpha + \sum_k \int d\mathbf{r} H_{ij}^k \delta\phi_k(\mathbf{r}) = 0 \quad , \tag{46}$$

where $H_{ij}^k \equiv \frac{\delta H_{ij}}{\delta \phi_k(\mathbf{r})}$. Division by dR_α yields

$$\frac{\partial H_{ij}}{\partial R_\alpha} - \epsilon_i^\alpha \delta_{ij} = -\sum_k \int d\mathbf{r} H_{ij}^k \phi_k^\alpha(\mathbf{r}) = -\sum_k \int d\mathbf{r} \int d\mathbf{r}' H_{ij}^k \delta(\mathbf{r} - \mathbf{r}') \phi_k^\alpha(\mathbf{r}') \quad . \quad (47)$$

On the rhs of Eq. (47) we have inserted a delta function, which we now express in terms of KS orbitals

$$\delta(\mathbf{r} - \mathbf{r}') = \sum_l \phi_l(\mathbf{r})\phi_l(\mathbf{r}') \quad . \quad (48)$$

Thus Eq. (47) becomes

$$\frac{\partial H_{ij}}{\partial R_\alpha} - \epsilon_i^\alpha \delta_{ij} = -\sum_{kl} H_{ij}^{kl} \phi_k^{\alpha l} \quad , \quad (49)$$

where

$$H_{ij}^{kl} \equiv \int d\mathbf{r} H_{ij}^k \phi_l(\mathbf{r})$$

$$= (\delta_{ik}\delta_{lj} + \delta_{jk}\delta_{li})\epsilon_l + 2n_k \int d\mathbf{r} \int d\mathbf{r}' \Gamma_{kl}(\mathbf{r}) f_{\text{H,xc}}(\mathbf{r},\mathbf{r}') \Gamma_{ij}(\mathbf{r}') \quad , \quad (50)$$

and

$$\phi_k^{\alpha l} \equiv \int d\mathbf{r} \phi_l(\mathbf{r}) \phi_k^\alpha(\mathbf{r}) \quad , \quad (51)$$

n_k being the number of electrons occupying orbital k.

Exploiting the symmetry of the nonadiabatic coupling matrix elements (Eq. (51)), i.e. $\phi_l^{\alpha k} = -\phi_k^{\alpha l}$ and therefore $\phi_l^{\alpha l} = 0$, Eq. (49) can be rewritten as

$$\frac{\partial H_{ij}}{\partial R_\alpha} = \sum_{l<k} D_{ij}^{lk} \phi_k^{\alpha l} \quad , (i < j) \quad (52)$$

and for the diagonal terms $(i = j)$

$$\epsilon_i^\alpha = \frac{\partial H_{ii}}{\partial R_\alpha} - \sum_{k<l} D_{ii}^{kl} \phi_k^{\alpha l} \quad , \quad (53)$$

where

$$D_{ij}^{lk} = H_{ij}^{lk} - H_{ij}^{kl} = (\delta_{il}\delta_{kj} + \delta_{ik}\delta_{lj})(\epsilon_k - \epsilon_l) + 2(n_k - n_l)K_{ij,lk} \quad . \quad (54)$$

With the definition in Eq. (54) Eq. (52) becomes

$$\frac{\partial H_{hp}}{\partial R_\alpha} = \sum_{p'h'} ((\epsilon_{p'} - \epsilon_{h'})\delta_{pp'}\delta_{hh'} + 4K_{p'h',ph})\phi_{h'}^{\alpha p'} \quad (55)$$

for particle-hole states, and

$$\frac{\partial H_{ij}}{\partial R_\alpha} = 4\sum_{ph} K_{ij,ph}\phi_h^{\alpha p} + (\epsilon_i - \epsilon_j)\phi_i^{\alpha j} \quad , (i < j, \ ij \ni ph) \quad (56)$$

for all remaining combinations. Eq. (56) allows us to express the nonadiabatic coupling elements between non-particle-hole states analytically as

$$\phi_i^{\alpha j} = \frac{\frac{\partial H_{ij}}{\partial R_\alpha} + 4 \sum_{ph} K_{ij,ph} \phi_h^{\alpha p}}{(\epsilon_i - \epsilon_j)} \quad , (i < j, \ ij \ni ph) \quad . \tag{57}$$

The system of linear equations (55) is first solved for the particle-hole nonadiabatic coupling elements $\phi_p^{\alpha h}$, which are then inserted into Eq. (57) to obtain the remaining, non-particle-hole, elements. The second term in the numerator of Eq. (57) is most conveniently evaluated by introducing the contracted density

$$\Gamma_3(\mathbf{r}) = \sum_{ph} \phi_p(\mathbf{r}) \phi_h(\mathbf{r}) \phi_h^{\alpha p} \quad . \tag{58}$$

Then

$$\sum_{ph} K_{ij,ph} \phi_p^{\alpha h} = \int d\mathbf{r} \int d\mathbf{r}' \Gamma_3(\mathbf{r}) f_{\mathrm{H,xc}}(\mathbf{r}, \mathbf{r}') \phi_i(\mathbf{r}') \phi_j(\mathbf{r}') \equiv K'_{ij} \quad . \tag{59}$$

Thus Eq. (57) becomes

$$\phi_j^{\alpha i} = \frac{\frac{\partial H_{ij}}{\partial R_\alpha} + 4 K'_{ij}}{(\epsilon_i - \epsilon_j)} \quad , (i < j, \ ij \ni ph) \quad . \tag{60}$$

Similarly the KS orbital energy gradients can now be obtained from the simplified Eq. (53)

$$\epsilon_i^\alpha = \frac{\partial H_{ii}}{\partial R_\alpha} + 4 K'_{ii} \quad . \tag{61}$$

Finally, the nuclear derivative of the KS orbital wave function is recovered by unfolding the nonadiabatic couplings

$$\phi_k^\alpha(\mathbf{r}) = \sum_l \phi_l(\mathbf{r}) \phi_k^{\alpha l} \quad . \tag{62}$$

Equations (1)–(31) have been implemented with periodic boundary conditions using a plane wave expansion of the KS MOs at the Γ point of the Brillouin zone. By making use of the periodic boundary conditions, the generalized densities Γ_1, Γ_2, Γ_3 and Γ_{ij} can be expanded in reciprocal space via the three-dimensional Fourier transform, e.g.

$$\Gamma_1(\mathbf{r}) = \sum_{\mathbf{G}} \Gamma_1(\mathbf{G}) \exp(i \mathbf{G} \mathbf{r}) \tag{63}$$

where $\mathbf{G}$ is the vector of the reciprocal lattice. The Hartree part of the matrix element $\int d\mathbf{r} \int d\mathbf{r}' \Gamma_1(\mathbf{r}) f_{\mathrm{H,xc}}(\mathbf{r}, \mathbf{r}') \Gamma_2(\mathbf{r}')$ and $\int d\mathbf{r} \int d\mathbf{r}' \Gamma_{kl}(\mathbf{r}) f_{\mathrm{H,xc}}(\mathbf{r}, \mathbf{r}') \Gamma_{ij}(\mathbf{r}')$ which enter the key equations (41) and (50), respectively, can be readily computed in reciprocal space, e.g.

$$\int d\mathbf{r} \int d\mathbf{r}' \Gamma_1(\mathbf{r}) \frac{1}{|\mathbf{r} - \mathbf{r}'|} \Gamma_2(\mathbf{r}') = \Omega \sum_{\mathbf{G} \neq 0} \frac{2\pi}{G^2} \Gamma_1(\mathbf{G}) \Gamma_2(\mathbf{G}) \quad , \tag{64}$$

whereas the exchange-correlation parts of the matrix elements are calculated via direct numerical integration over grid in coordinate space.

active space	ΔE_{KS}	1o/1v	5o/1v	5o/5v	5o/50v	5o/100v
exc. energy	8.39	9.47	9.40	9.40	9.33	9.29

Table 1. Dependence of N_2 TDLDA excitation energy ($^1\Pi_g$, $3\sigma_g \to 1\pi_g$) in eV using plane waves (p.w.) with a 70 Ry cutoff in a 10 a_0 periodic box on the number of occupied (o) and virtual (v) Kohn-Sham orbitals included in the active space. ΔE_{KS} is the unperturbed Kohn-Sham energy difference.

3   Example Calculations

In this section, we present some (test) results for excitation energies and gradients from the TDDFT implementations described in Refs. 43, 44. All calculations were performed with the CPMD package[50] employing periodic boundary conditions and a plane wave (PW) basis set in conjunction with Troullier-Martins normconserving pseudopotentials[51].

The central idea underlying this active space (AS) approach originates from the observation that excitation energies for a large number of electronic transitions exhibit only a minor dependence on the size of the response matrix (Eq. 27)). This is illustrated in Table 1 for the $3\sigma_g \to 1\pi_g$ transition of N_2. A simple two-state HOMO–LUMO response calculation is seen to give an excitation energy which is less than 0.2 eV away from an extended treatment including all 5 occupied and 100 virtual MOs. Generally, such behavior is to be expected for excitations which can be characterized by only a few low-lying one-electron transitions without higher-lying continuum states mixing in.

Table 2 lists the first eight excitation energies of N_2 comparing the AS-PW results (30 a.u. unit cell, 70 Ry cutoff, AS consisting of 5 h and 85 p states) to atomic basis set studies as well as experimental data. We observe satisfactory agreement, the largest difference being 0.19 eV for the $3\sigma_g \to 1\pi_g$ transition.

As a further example, our results for H_2CO in a fcc lattice (30 a.u. unit cell, 70 Ry cutoff, AS contained 6 h and 70 p states) are presented in Table 3. Again, there is reason-

Transition	TDLDA					CCSD	Exp.
	ref.[22]	ref.[37]	ref.[31]	ref.[52]	AS-PW[43]	ref.[53]	ref.[54]
($^1\Delta_u$) $1\pi_u \to 1\pi_g$	10.22	10.23	10.21	10.20	10.25	10.54	10.27
($^1\Sigma_u^-$) $1\pi_u \to 1\pi_g$	9.65	9.68	9.64	9.63	9.73	10.09	9.92
($^1\Pi_g$) $3\sigma_g \to 1\pi_g$	9.05	9.07	9.04	9.04	9.23	9.27	9.31
($^3\Pi_u$) $2\sigma_u \to 1\pi_g$	10.36	10.37	10.36	10.36	10.45	11.19	11.19
($^3\Sigma_u^-$) $1\pi_u \to 1\pi_g$	9.65	9.68	9.64	9.63	9.73	9.86	9.67
($^3\Delta_u$) $1\pi_u \to 1\pi_g$	8.82	8.84	8.82	8.80	8.92	8.93	8.88
($^3\Pi_g$) $3\sigma_g \to 1\pi_g$	7.54	7.58	7.54	7.53	7.66	8.05	8.04
($^3\Sigma_u^+$) $1\pi_u \to 1\pi_g$	7.86	7.90	7.86	7.84	7.99	7.56	7.75
polarizability [a.u.]	-	12.27	12.17	12.11	12.6		11.74

Table 2. Comparison of AS-PW N_2 excitation energies in eV to other TDLDA results obtained with atomic sets, CCSD, and experiment. In the last row, sum-over-states values for the mean static polarizability are compared to the experimental number.

| Transition | TDLDA | | | | CASPT2 | Exp. |
	ref.[22]	ref.[31]	AS-PW[43]	AS-PW(AC)[43]	ref.[55]	ref.[56,57]
$^1A_2$ $(n \to \pi^*)$	3.64	3.68	3.68	3.69	3.91	3.94
$^3A_2$ $(n \to \pi^*)$	3.02	3.06	3.08	3.08	3.48	3.50
$^3A_1$ $(\pi \to \pi^*)$	6.11	6.24	6.38	6.39	5.99	5.53
$^1B_1$ $(\sigma \to \pi^*)$	8.70	8.79	8.94	8.94	9.09	8.68
$^3B_2$ $(n \to 3s)$	5.86	5.78	5.65	6.56	-	6.83
$^1B_2$ $(n \to 3s)$	5.93	5.82	5.76	6.89	7.30	7.09
$^3A_1$ $(n \to 3p)$	-	6.48	6.73	7.59	-	7.79
$^1A_1$ $(n \to 3p)$	6.79	6.49	6.93	7.83	8.09	7.97

Table 3. Comparison of H_2CO AS-PW excitation energies in eV with and without asymptotic correction (AC) to literature TDLDA results obtained with a gaussian set and experiment.

able agreement between the different LDA studies. The CASPT2 excitation energies are, however, much closer to the experimental values than the TDLDA results. Moreover, inspecting the data for the transitions to the $3s$ and $3p$ Rydberg orbitals the deficiency of the LDA exchange-correlation potential at long range becomes apparent. These problems persist for most GGA's. In contrast, employing the asymptotic correction proposed by Tozer and Handy[31] these excitation energies can be drastically improved as shown in Table 3.

In our final example, we go beyond the static, zero temperature description. Figure 1 depicts an average photoabsorption spectrum of formamide obtained from the instantaneous spectra of 11 molecular configurations sampled from a CPMD run at 300 K. Although many more configurations are needed to obtain a converged spectrum, we are able to reproduce the most important features of the experimental photoabsorption spectrum. The W band (see Table 4 for a summary of this historic nomenclature) resulting from the $n \to \pi^*$ transition has been found to have a maximum around 5.8 eV[58]. Gingell et al.[58] have associated the R_1 band between 6.2 and 7.0 eV with transitions from the n and π orbitals to the $3s$ Rydberg orbital which is supposed to be mixed with a σ^* valence orbital. The main absorption peak V_1 with a maximum at roughly 7.4 eV has traditionally been linked to the $\pi_2 \to \pi^*$ transition, whereas the sharp structure on its high-energy side has been assigned to transitions to $3p$ Rydberg orbitals[58]. There remains considerable doubt regarding the origin of the broad band, Q, around 9.2 eV, which, for a long time, was thought to be due to the $\pi_1 \to \pi^*$ transition[59]. Gingell et al.[58] have interpreted this peak as a superposition of a large number of Rydberg states.

Our theoretical LDA absorption spectrum in Figure 1 is seen to agree overall quite well with the VUV curve, only the low-energy side of the main peak seemingly being somewhat overestimated. However, analyzing the individual excitations at equilibrium geometry listed in Table 4, it becomes clear that use of the asymptotically corrected LDA exchange-correlation potential corrects for this discrepancy. According to our calculations, the R_1 band then unambiguously arises from $n \to 3s$ and $\pi \to 3s$ excitations. We cannot confirm, however, any involvement of a σ^* valence orbital as previously assumed[58]. Instead we observe a small contribution (roughly 5% in the asymptotically corrected case) from the $\pi_2 \to \pi^*$ transition. Our calculations further reveal that all the sharp structure of

transition	AS-PW[43]	AS-PW(AC)[43]	HCTH(AC)[60]	CASPT2[61]	Exp.[58]
$n \rightarrow \pi^*$	5.27	5.29	5.43	5.61	5.8 (W)
$n \rightarrow 3s$	5.56	6.27	6.30	6.59	6.35 (R$_1$)
$\pi \rightarrow 3s$	6.28	7.09	7.03	6.52	
$n \rightarrow 3p$	6.44	7.22	7.09	7.31	7.7 (R$_2$)
$\pi \rightarrow 3p$	7.18	7.91	7.76	7.04	
$\pi \rightarrow \pi^*$	7.80	7.67	7.58	7.41	7.4 (V$_1$)

Table 4. Comparison of formamide equilibrium geometry AS-PW excitation energies in eV using LDA with and without asymptotic correction (AC) to literature data.

the main peak is due to excitations from n to $3p$ orbitals, generally being more intense by one order of magnitude compared with their $\pi_2 \rightarrow 3p$ equivalents.

The most intense line found with LDA(AC) is at 7.67 eV and its character is a mixture of 37% $\pi_2 \rightarrow \pi^*$ and 63% excitations from the n or π_2 valence to $3p$ or $3d$ Rydberg orbitals. A small $\pi_2 \rightarrow \pi^*$ contribution can also be detected in our calculated Q band, which otherwise predominantly results from $n \rightarrow 3d$ transitions.

We would like to point out that our LDA(AC) results are in accord with the HCTH(AC) values of Handy[60]. On the other hand, the CASPT2 results of Serrano-Andrés and Fülscher[61] show larger differences; in particular the energetic ordering of excitation from the n and π_2 orbitals seems to be reversed.
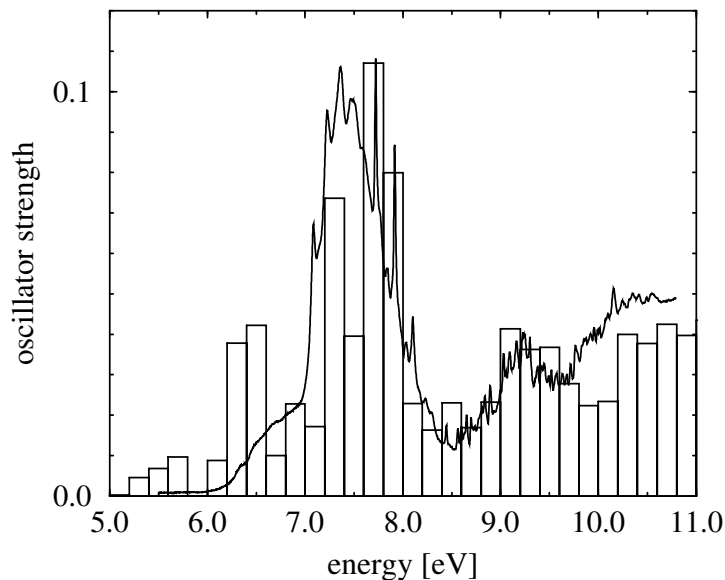

Figure 1. Theoretical room temperature photoabsorption spectrum of formamide obtained from TDLDA calculations (white bars) compared to the experimental VUV data of Gingell et al..
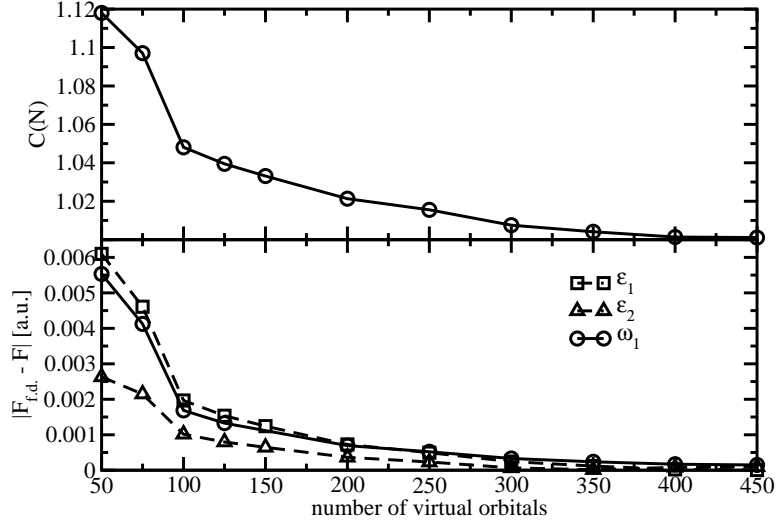
Figure 2. Upper panel: The integral in Eq. (65) as a function of the number of virtual orbitals included in the active space. Lower panel: Absolute deviation of finite difference and analytic derivatives of the KS HOMO and LUMO energies and the first singlet excitation energy of H_2 at a bond length of 1.0 a.u. as a function of the number of virtual KS orbitals included in the active space. The calculations were carried out in a cubic box of length 6 a.u. with periodic boundary conditions and a plane wave cutoff of 40 Ry.

In the following we shall illustrate the performance and the convergence behavior of the implicit differentiation method[44] (cf. Section 2.3.2) for nuclear gradients.

The upper panel of Figure 2 displays the completeness of the active space as a function of the number of virtual KS orbitals included in the space. The integral

$$C(N) = \int d\mathbf{r} \sum_{i=1}^{N} \phi_i(\mathbf{r})\phi_i(0) \tag{65}$$

was used as a measure of completeness of the active space. It becomes unity when the active space of KS orbitals is complete, i.e. when the total number of the KS orbitals (virtual and occupied) equals the number of plane waves used to solve the KS equations. The total number of plane waves is 925 for the 6 a.u. cubic box and 40 Ry plane wave cutoff. With 450 virtual orbitals included the active space is almost complete and the value of the integral (Eq. (65)) deviates from unity by approximately 10^{-3} which is already comparable with the accuracy of the numerical integration. The lower panel of Figure 2 shows the absolute deviation of the analytic derivatives from the respective finite difference values for the the first singlet excitation energy, ω_1, as well as the HOMO and LUMO KS orbital energies, ϵ_1 and ϵ_2, of H_2 at a bond length of 1.0 a.u. as a function of the number of virtual KS orbitals included in the active space. The absolute deviation in analytical gradients vanishes rapidly as the number of virtual orbitals is increased and the errors in the analytical gradients of different states generally show the same patterns in the dependence upon the number of virtual orbitals included in the active space.

Figure 3 shows the absolute deviation of the analytical derivative from the respective finite difference value as a function of the size of the active space for the first three KS
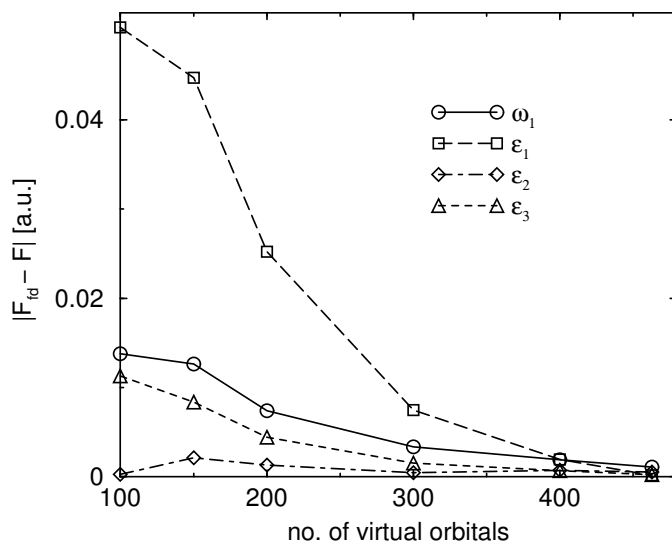
13

Figure 3. Absolute deviation of the analytic derivatives from the respective finite difference values for the the first singlet excitation energy, ω_1, as well as the three lowest KS orbital energies, ϵ_i ($i = 1, 2, 3$), of N_2 at a bond length of 2.0 a.u. as a function of the number of virtual KS orbitals included in the active space. The calculations were carried out in a cubic box of length 6 a.u. with periodic boundary conditions and a plane wave cutoff of 40 Ry.

orbital energies ϵ_i ($i = 1, 2, 3$) as well as the lowest response matrix eigenvalue ω_1 of the N_2 molecule. The errors of the analytical gradients are seen to decrease rapidly as the number of orbitals included in the active space approaches the number of plane wave basis functions (in this case 925 plane waves). For the largest active space the deviations of all energies are of the order of 10^{-3} or smaller. At this point, the accuracy of the analytical derivatives is hard to assess because the finite difference reference values are also subjected to numerical errors.

To test the practical value of our derivatives, we have performed geometry optimizations of N_2 in the first excited state ($8 \times 5.6 \times 5.6$ a.u. box, 40 Ry plane-wave cutoff, i.e. 600 basis functions). When we include only 100 virtual orbitals in the active space, we obtain a bond length of 2.44 a.u., which deviates by 0.02 a.u. from the value of 2.42 a.u. determined by a series of single point energy calculations. Upon increasing the number of virtual states to 200, the optimized bond length comes out as 2.42 a.u., correct to two decimal places. Our test calculations illustrate how the size of the active space may be adjusted to achieve any desired level of accuracy. For many practical purposes it will be sufficient to work with a reduced active space which is significantly smaller than the total number of basis functions.

We would like to emphasize that the method described here is capable of providing additional information beyond excited state energy gradients. Figure 4 shows, for instance, the nonadiabatic coupling strength between the second and third KS orbitals, ϕ_2 and ϕ_3, for the H_2 molecule as a function of its bond length. The nonadiabatic coupling values obtained from Eq. (60) exhibit a singularity at the crossing point between the two KS
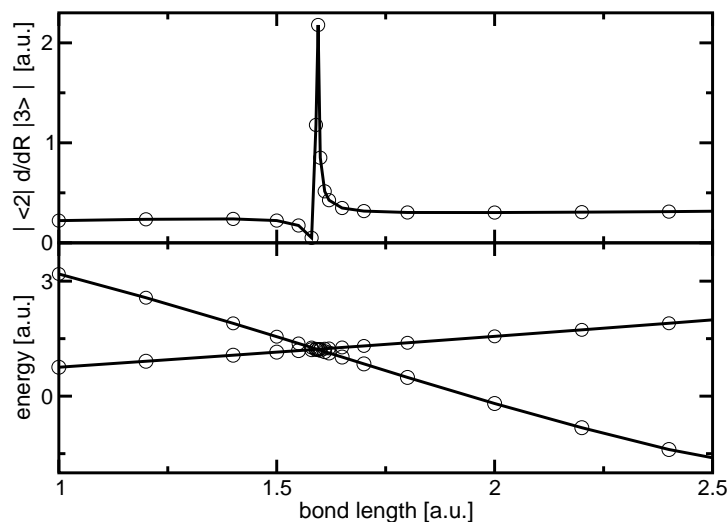
Figure 4. Upper panel: Absolute value of the nonadiabatic coupling matrix element between the KS orbitals ϕ_2 and ϕ_3 along the molecular axis of H_2 as a function of the bond length. Lower panel: KS orbital energies, ϵ_2 and ϵ_3 of H_2 as a function of bond length. The calculations were carried out in a periodic orthorhombic box of size $8 \times 5.6 \times 5.6$ a.u.[3] using a plane wave cutoff of 40 Ry.

orbital energies, as one would expect due to the KS energy difference in the denominator. This feature of our formalism may be exploited in future applications of TDDFT beyond the Born-Oppenheimer approximation.

Acknowledgements

References

1. T. Ziegler, A. Rauk, and E. J. Baerends. *Theor. Chim. Acta*, 43:261, 1977.
2. C. Daul. *Int. J. Quantum Chem.*, 52:867, 1994.
3. T. Ziegler. *Chem. Rev.*, 91:651, 1991.
4. U. von Barth. *Phys. Rev. A*, 20:1693, 1979.
5. B. I. Dunlap. *Chem. Phys.*, 125:89, 1988.
6. A. C. Stückl, C. A. Daul, and H. U. Güdel. *Int. J. Quantum Chem.*, 61:579, 1997.
7. I. Frank, J. Hutter, D. Marx, and M. Parrinello. *J. Chem. Phys.*, 108:4060, 1998.
8. J. Gräfenstein, E. Kraka, and D. Cremer. *Chem. Phys. Lett.*, 288:593, 1998.
9. J. Gräfenstein and D. Cremer. *Phys. Chem. Chem. Phys.*, 2:2091, 2000.
10. M. Filatov and S. Shaik. *Chem. Phys. Lett.*, 288:689, 1998.
11. M. Filatov and S. Shaik. *J. Chem. Phys.*, 110:116, 1999.
12. M. Filatov and S. Shaik. *Chem. Phys. Lett.*, 304:429, 1999.

13. S. Grimm, C. Nonnenberg, and I. Frank. *J. Chem. Phys.*, 119:11574, 2003. *ibid.* **119**, (2003) 11585.

14. E. Runge and E. K. U. Gross. *Phys. Rev. Lett.*, 52:997, 1984.

15. J. Theilhaber. *Phys. Rev. B*, 46:12990, 1992.

16. E. K. U. Gross, J. F. Dobson, and M. Petersilka. In R. F. Nastajewski, editor, *Density Functional Theory II*, Topics in Current Chemistry. Springer, Heidelberg, 1996.

17. U. Saalmann and R. Schmidt. *Z. Phys. D*, 38:153, 1996.

18. U. Saalmann and R. Schmidt. *Phys. Rev. Lett.*, 80:3213, 1998.

19. T. Kunert and R. Schmidt. *Phys. Rev. Lett.*, 86:5258, 2001.

20. B. Torralva, T. A. Niehaus, M. Elstner, S. Suhai, Th. Frauenheim, and R. E. Allen. *Phys. Rev. B*, 64:153105, 2001.

21. M. E. Casida. In D. P. Chong, editor, *Recent Advances in Density-Functional Methods*, page 155. World Scientific, Singapore, 1995.

22. R. Bauernschmitt and R. Ahlrichs. *Chem. Phys. Lett.*, 256:454, 1996.

23. M. A. L. Marques and E. K. U. Gross. *Annu. Rev. Phys. Chem.*, 55:427, 2004.

24. K. Burke, J. Werschnik, and E. K. U. Gross. *J. Chem. Phys.*, 123:062206, 2005.

25. N. T. Maitra, K. Burke, H. Appel, E. K. U. Gross, and R. van Leeuwen. In K. D. Sen, editor, *Reviews in Modern Quantum Chemistry: A Celebration of the Contributions of R. G. Parr*, volume 2, page 1186. World-Scientific, Singapore, 2002.

26. D. J. Tozer and N. C. Handy. *Phys. Chem. Chem. Phys.*, 2:2117, 2000.

27. O. Gritsenko and E. J. Baerends. *J. Chem. Phys.*, 121:655, 2004.

28. L. Bernasconi, M. Sprik, and J. Hutter. *Chem. Phys. Lett.*, 394:141, 2004.

29. A. Dreuw, J. L. Weisman, and M. Head-Gordon. *J. Chem. Phys.*, 119:2943, 2003.

30. M. E. Casida, F. Gutierrez, J. Guan, F.-X. Gadea, D. Salahub, and J.-P. Daudey. *J. Chem. Phys.*, 113:7062, 2000.

31. D. J. Tozer and N. C. Handy. *J. Chem. Phys.*, 109:10180, 1998.

32. M. E. Casida, C. Jamorski, K. C. Casida, and D. R. Salahub. *J. Chem. Phys.*, 108:4439, 1998.

33. M. E. Casida and D. R. Salahub. *J. Chem. Phys.*, 113:8918, 2000.

34. S. Hirata, C.-G. Zhan, E. Aprà, T. L. Windus, and D. A. Dixon. *J. Phys. Chem. A*, 107:10154, 2003.

35. S. Hirata and M. Head-Gordon. *Chem. Phys. Lett.*, 302:375, 1999.

36. H. Appel, E. K. U. Gross, and K. Burke. *Phys. Rev. Lett.*, 90:043005, 2003.

37. P. R. T. Schipper, O. V. Gritsenko, S. J. A van Gisbergen, and E. J. Baerends. *J. Chem. Phys.*, 112:1344, 2000.

38. H. H. Neinze, A. Görling, and N. Rösch. *J. Chem. Phys.*, 113:2088, 2000.

39. C. van Caillie and R. D. Amos. *Chem. Phys. Lett.*, 308:249, 1999.

40. C. van Caillie and R. D. Amos. *Chem. Phys. Lett.*, 317:159, 2000.

41. F. Furche and R. Ahlrichs. *J. Chem. Phys,*, 117:7433, 2002.

42. J. Hutter. *J. Chem. Phys.*, 118:3928, 2003.

43. N. L. Doltsinis and M. Sprik. *Chem. Phys. Lett.*, 330:563, 2000.

44. N. L. Doltsinis and D. Kosov. *J. Chem. Phys.*, 122:144101, 2005.

45. E. R. Bittner and D. S. Kosov. *J. Chem. Phys.*, 110:6645, 1999.

46. P. Hohenberg and W. Kohn. *Phys. Rev. B*, 136:864, 1964.

47. E. K. U. Gross and W. Kohn. *Adv. Quant. Chem.*, 21:255, 1990.

48. M. Petersilka, U. J. Grossmann, and E. K. U. Gross. *Phys. Rev. Lett.*, 76:1212, 1996.

49. P. Jørgensen and J. Simons. *Second Quantization Based Methods in Quantum Chemistry*. Academic, New York, 1981.

50. `CPMD 3.4`: J. Hutter, P. Ballone, M. Bernasconi, P. Focher, E. Fois, S. Goedecker, D. Marx, M. Parrinello, and M. Tuckerman; MPI für Festkörperforschung, Stuttgart and IBM Zurich Research Laboratory.

51. N. Troullier and J. L. Martins. *Phys. Rev. B*, 43:1993, 1991.

52. C. Jamorski, M. E. Casida, and D. R. Salahub. *J. Chem. Phys.*, 104:5134, 1996.

53. S. B. Ben-Shlomo and U. Kaldor. *J. Chem. Phys.*, 92:3680, 1990.

54. J. Oddershede, N. E. Grüner, and G. H. F. Diercksen. *Chem. Phys.*, 97:303, 1985.

55. M. Merchán and B. O. Roos. *Theor. Chim. Acta*, 92:227, 1995.

56. D. J. Clouthier and D. A. Ramsay. *Annu. Rev. Phys. Chem.*, 34:31, 1983.

57. S. Taylor, D. G. Wilden, and J. Comer. *Chem. Phys.*, 70:291, 1982.

58. J. M. Gingell, N. J. Mason, H. Zhao, I. C. Walker, and M. R. F. Siggel. *Chem. Phys.*, 220:191, 1997.

59. H. D. Hunt and W. T. Simpson. *J. Am. Chem. Soc.*, 75:4540, 1953.

60. N. C. Handy. private communication.

61. L. Serrano-Andrés and M. P. Fülscher. *J. Am. Chem. Soc.*, 118:12199, 1996.